Applied Catalysis B: Environmental 225 (2018) 84–90

Contents lists available at ScienceDirect

Applied Catalysis B: Environmental

journal homepage: www.elsevier.com/locate/apcatb

Hollow $PdCu_2$@Pt core@shell nanoparticles with ordered intermetallic cores as efficient and durable oxygen reduction reaction electrocatalysts

Hee-Young Park[a,1], Jin Hoo Park[b,1], Pil Kim[b,*], Sung Jong Yoo[a,c,d,*]

[a] Fuel Cell Research Center, Korea Institute of Science and Technology, 5 Hwarangno 14-gil, Seongbuk-gu, Seoul 02792, Republic of Korea
[b] School of Semiconductor and Chemical Engineering, Chonbuk National University, Baekje-daero 567, Jeonju 54896, Republic of Korea
[c] Division of Energy and Environment Technology, KIST School, Korea University of Science and Technology, 5 Hwarang-ro 14-gil, Seongbuk-gu, Seoul 02792, Republic of Korea
[d] KHU-KIST Department of Converging Science and Technology, Kyung Hee University, 26, Kyungheedae-ro, Dongdaemun-gu, Seoul 02447, Republic of Korea

ARTICLE INFO

Keywords:
Polymer electrolyte membrane fuel cell
Oxygen reduction reaction
Hollow nanoparticles
$PdCu_2$@Pt core@shell
Ordered intermetallic core

ABSTRACT

Carbon-supported hollow $PdCu_2$@Pt core@shell nanoparticles with ordered intermetallic cores were prepared as an efficient and durable oxygen reduction reaction (ORR) electrocatalyst for polymer electrolyte membrane fuel cells (PEMFCs). $PdCu_2$ cores prepared using a chemical reduction method were thermally treated to produce ordered intermetallic structures. A Pt shell was then deposited via a galvanic displacement process. The effect of the galvanic displacement conditions on the properties and structure of the obtained core–shell nanoparticles was investigated by varying the solution pH and anion concentration. Acidic conditions and low Cl^- concentrations were found to provide a uniform Pt layer with a hollow core, while maintaining the ordered intermetallic core structure. These hollow $PdCu_2$@Pt core@shell nanoparticles showed high activity and stability for ORR electrocatalysis in PEMFCs.

1. Introduction

Efficient electrocatalysis of the oxygen reduction reaction (ORR) is crucial as sluggish reactions result in heavy consumption of Pt-based electrocatalysts, which is considered a major obstacle for widespread utilization of polymer electrolyte membrane fuel cells (PEMFCs). As ORR electrocatalysis occurs on Pt surfaces, strategies to enhance ORR activity while reducing Pt consumption are straightforward: increase the turnover frequency of surface Pt atoms and maximize the fraction of surface Pt atoms. To enhance the turnover frequency of surface Pt atoms, alloying with transition metals, such as Ni, Co, Y, and Sc, has been investigated [1–4]. The enhanced turnover frequency of Pt alloys with transition metals (by 3–7 times) is often explained by the weaker bond strength of the reaction intermediate (OH_{ad}) [3]. Further, it has been suggested that the fraction of surface Pt atoms could be maximized by depositing a few layers of Pt atoms on foreign nanoparticles to achieve “core@shell” structures [5–7]. In particular, carefully selected cores were reported to enhance the turnover frequency as well as the surface fraction of Pt atoms [5,7]. Pd and Pd alloy cores enhance the turnover frequency of surface Pt atoms by 2.5–5 times, probably because of lattice contraction in the Pt layers [8–15]. As contraction of the Pt crystal lattice lowers the d-band center of Pt atoms, the bond strength of OH_{ad} decreases and, thereby, the ORR activity increases [8].

Several approaches have been introduced to form surface Pt layers, including galvanic displacement of Cu with Pt [8–14], chemical reduction of Pt, and spontaneous deposition of Pt. Galvanic displacement of Cu with Pt has been widely utilized to produce Pt layers because this process allows easy manipulation of surface structure and composition [11,13,16]. As the standard reduction potential of Cu (0.337 V) is more negative than that of Pt (0.735 V), $PtCl_6^{2-}$ is expected to replace Cu atoms. Furthermore, if Cu atoms are present in the nanoparticles as well as on the surface of the nanoparticles, continuous replacement of Cu with Pt has been reported to generate porous cores and Pt-rich surfaces [11,16].

Among the various possible architectures, we are interested in Pt-decorated Pd–Cu alloys (Pd_xCu_y@Pt), as Pt lattice contraction by Pd_xCu_y cores should enhance the turnover frequency of Pt atoms and surface Pt layers should be easily formed by galvanic replacement of Cu in the core particles with Pt [9–11,13,16]. If the core nanoparticles do not contain Cu atoms, an additional process to make sacrificial Cu layers, e.g., electrodeposition, is required for the galvanic displacement process [8,12,14]. Despite numerous studies on Pd_xCu_y@Pd core@shell nanoparticles for ORR electrocatalysis [9–11,13,16], there has been little investigation of the effect of chemical environment on the

* Corresponding authors.
E-mail addresses: kimpil1@chonbuk.ac.kr (P. Kim), ysj@kist.re.kr (S.J. Yoo).
[1] Dr. Hee-Young Park and Dr. Jin Hoo Park are the co-authors for this article.

https://doi.org/10.1016/j.apcatb.2017.11.052
Received 16 May 2017; Received in revised form 4 September 2017; Accepted 20 November 2017
Available online 22 November 2017

structure and electrochemical properties of the obtained Pd_xCu_y@Pt nanoparticles. In particular, to the best of our knowledge, although ordered intermetallic structures are beneficial for high durability [17–19], the ORR activity and stability of Pd_xCu_y@Pt nanoparticles with ordered intermetallic Pd_xCu_y cores has not been reported.

In this study, we developed highly efficient and durable hollow $PdCu_2$@Pt core@shell electrocatalysts with ordered intermetallic cores. As $PdCu_2$ cores provide a unique ordered intermetallic structure, both high stability and high activity were expected. The effect of galvanic displacement conditions, such as pH and Cl^- concentration, on the structure and electrochemical properties of $PdCu_2$@Pt nanoparticles were examined.

2. Experimental

2.1. Preparation of electrocatalysts

As the core material, carbon-supported $PdCu_2$ nanoparticles ($PdCu_2$) were prepared via the chemical reduction of $Pd(NO_3)_2$ (Kojima Chemicals) and $Cu(NO_3)_2$ (Shinyo Pure Chemicals) in a mixture of deionized water (18.3 MΩ cm) and carbon support (Vulcan XC72, Cabot), followed by heat treatment at 500 °C under a mixture of hydrogen and nitrogen gases (10/90, v/v) for 2 h. The weight composition of metal nanoparticles in the core material was 30%. A sodium borohydride (Sigma Aldrich) solution (0.21 mM) was utilized as the reducing agent. To obtain core@shell electrocatalysts, $PdCu_2$/C was dispersed in deionized water and 10 mL of Pt precursor ($H_2PtCl_6{\cdot}xH_2O$, Kojima Chemicals) solution was introduced to the mixture under an inert (N_2) atmosphere. The atomic ratio of Pd and Pt was adjusted to 2. The mixture was stirred for 1 h and then filtered and washed with deionized water to isolate the black precipitate. The precipitate was then dried in a convection oven at 100 °C for approximately 12 h ($PdCu_2$@Pt-H). To investigate the effect of the galvanic displacement conditions on the structure and electrochemical properties of the obtained $PdCu_2$@Pt electrocatalysts, $PdCu_2$-Pt-K and $PdCu_2$-Pt-K-HCl samples were prepared using the same procedure as for $PdCu_2$@Pt-H by replacing the $H_2PtCl_6{\cdot}xH_2O$ solution with a K_2PtCl_6 (Sigma Aldrich) solution and a K_2PtCl_6 in 0.05 M HCl (Sigma Aldrich) solution, respectively (Scheme. 1).

2.2. Physicochemical analysis

Transmission electron microscopy (TEM) images, scanning transmission electron microscopy (STEM) images, and energy dispersive spectroscopy (EDS) line profiles were obtained using a JEOL-2010 microscope (JEOL). The X-ray diffraction (XRD) patterns of the electrocatalysts were recorded using an X'pert Powder diffractometer (PANanalytical). The atomic compositions of the electrocatalysts were determined using an ICPS-7510 inductively coupled plasma (ICP) emission spectrometer (Shimadzu). X-ray photoelectron spectroscopy (XPS) analysis was carried out using a K-Alpha ESCA system (Thermo Scientific).

2.3. Electrochemical analysis

Electrochemical analysis of the electrocatalysts was conducted using a conventional three-electrode setup with a CHI700C electrochemical analyzer (CH Instruments). An electrocatalyst-coated rotating ring disk electrode (RRDE) with a glassy carbon disk (0.2475 cm^2) and Pt ring electrode (Pine Instruments) was utilized as the working electrode. To prepare the working electrode, a mixture of electrocatalyst, Nafion solution, and isopropanol was dropped onto the RRDE and then dried under an air atmosphere. A Ag/AgCl reference electrode (BASi) and a Pt wire served as the reference and counter electrodes, respectively. ORR polarization curves were recorded in O_2-saturated 0.1 M $HClO_4$ at a rotating speed of 1600 rpm. To evaluate the stability of the electrocatalysts, ORR polarization curves were obtained after potential cycling between 0.6 and 1.0 V for 10,000 cycles at a scan rate of 50 mV in Ar-saturated 0.1 M $HClO_4$. Cyclic voltammograms of the electrocatalysts were recorded in Ar-saturated 0.1 M $HClO_4$ at a scan rate of 20 mV s^{-1}.

3. Results and discussion

3.1. Effect of galvanic displacement conditions on the morphology and crystalline structure of the electrocatalysts

Fig. 1 shows TEM and STEM images and EDS line scan profiles of the $PdCu_2$ cores and the $PdCu_2$@Pt-H, $PdCu_2$-Pt-K, and $PdCu_2$-Pt-K-HCl electrocatalysts. The $PdCu_2$ cores are spherical nanoparticles with

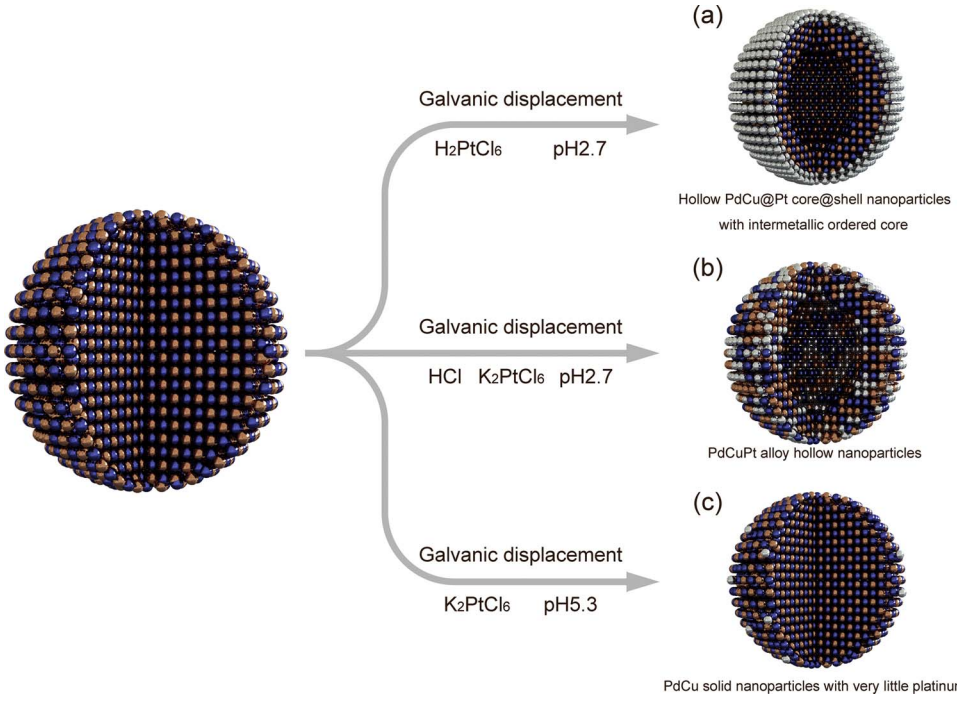

Scheme 1. Schematic illustration of the structures of (a) $PdCu_2$@Pt-H, (b) $PdCu_2$-Pt-K-HCl, and (c) $PdCu_2$-Pt-K electrocatalysts.

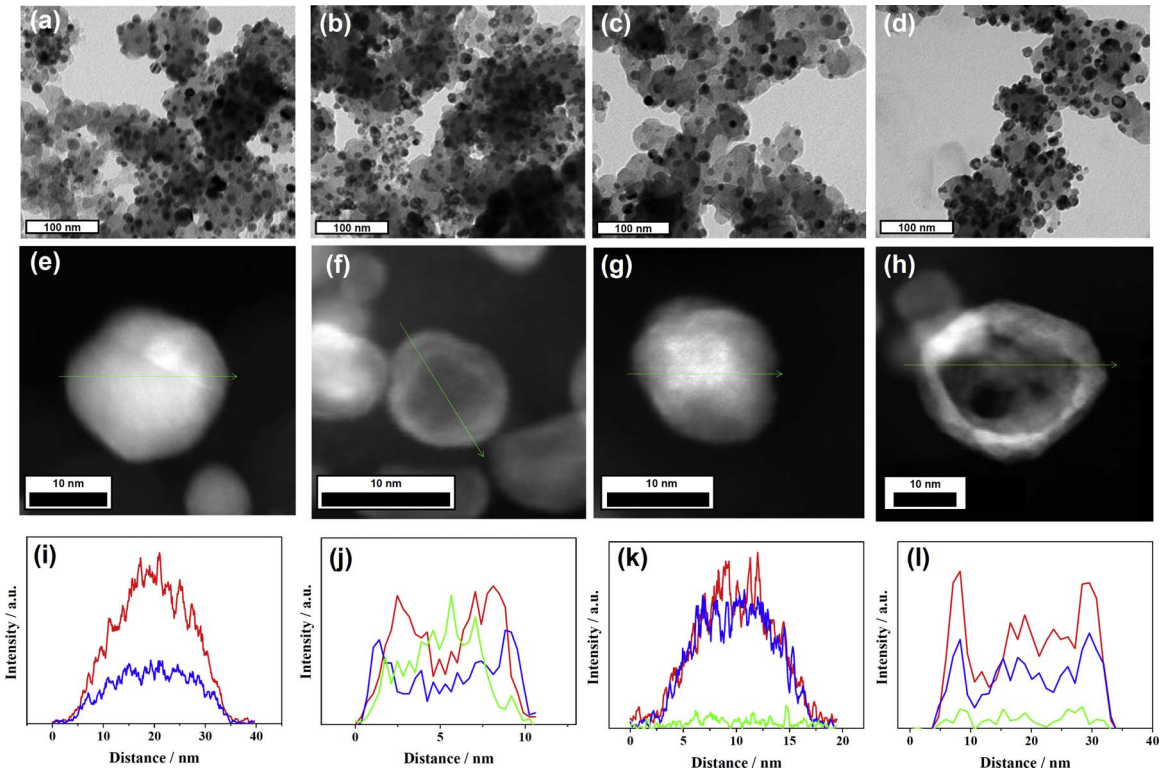

Fig. 1. TEM (a–d) and STEM (e–h) images and EDS line scan profiles (i–l) of $PdCu_2$ (a, e, i), $PdCu_2$@Pt-H (b, f, j), $PdCu_2$-Pt-K (c, g, k), and $PdCu_2$-Pt-K-HCl (d, h, l). Blue, green, and red lines in the EDS line scan profiles correspond to signals from Cu, Pt, and Pd atoms, respectively. (For interpretation of the references to colour in this figure legend, the reader is referred to the web version of this article.).

diameters of 15–25 nm (Fig. 1a). The STEM image and corresponding EDS analysis of the cores (Fig. 1e, 1i and S1) revealed that Pd and Cu atoms are uniformly mixed in the $PdCu_2$ nanoparticles. The $PdCu_2$@Pt-H sample (Fig. 1b) exhibited hollow structures, as shown in the representative STEM image in Fig. 1f. The corresponding EDS line scan profile revealed that nanoparticles in the $PdCu_2$@Pt-H sample have an outer Pt-rich layer and a Pd- and Cu-rich inner shell (Fig. 1j). The Pt-rich layer was consistently observed in $PdCu_2$@Pt-H samples, although some $PdCu_2$@Pt nanoparticles exhibited nanoporous structures (Fig. S2). Conversely, nanoparticles in the $PdCu_2$-Pt-K sample have few Pt layers and a solid core, as evidenced by the TEM and STEM images (Fig. 1c and 1 g) and EDS line scan profile (Fig. 1k). Since the only difference in the Pt shell deposition conditions for $PdCu_2$@Pt-H and $PdCu_2$-Pt-K is the Pt precursor, the differences in the obtained structures are due to the Pt precursor. We conjecture that these differences result from variations in the pH during deposition of the Pt shell. The Pourbaix diagram of Cu indicates that Cu_2O and CuO are stable in neutral solution, whereas dissolved forms, such as Cu^{2+}, are stable in acidic conditions [20]. Thus, with the K_2PtCl_6 precursor, replacement of Cu with Pt may be hindered by CuO_x formation. This suggestion is supported by the fact that hollow-structured $PdCu_2$@Pt nanoparticles were obtained when the pH of the solution was adjusted to 2.7 by the addition of HCl ($PdCu_2$-Pt-K-HCl) (Fig. 1d and h). Notably, the EDS line scan profile of $PdCu_2$-Pt-K-HCl shows a virtually even distribution of Pt and Pd in the shell (Fig. 1l), whereas that of $PdCu_2$@Pt-H indicates the formation of surface Pt layers (Fig. 1).

The XRD pattern of $PdCu_2$/C shows that the $PdCu_2$ cores are a mixture of disordered face-centered cubic (FCC) and ordered intermetallic body-centered cubic (BCC) crystals (Fig. 2a), which is in good agreement with the phase diagram of Pd–Cu alloys [21]. The sizes of the FCC and BCC crystals were calculated as 4.9 and 9.2 nm, respectively, using the Scherrer equation and the peak broadening of the (220) diffraction for FCC crystals and the (211) diffraction for BCC crystals. As the size of the core particles observed in the TEM and STEM images was around 3–5 times larger than that of the FCC crystal and around 1.5–2.5 times larger than that of the BCC crystal, the majority of the $PdCu_2$ cores are considered as polycrystalline.

The crystal structure of $PdCu_2$@Pt-H is similar to that of the $PdCu_2$ core, although the peak position of the (220) plane diffraction of the FCC crystal is negatively shifted by 0.84°, probably owing to Cu dissolution (Fig. 2b). Notably, the peak position of the (211) plane diffraction of the BCC crystal in $PdCu_2$@Pt-H did not change significantly. These results suggest that during galvanic displacement, Cu dissolution occurs from the FCC crystals rather than the BCC crystals. As diffraction peaks corresponding to Pt are hardly observed for $PdCu_2$@Pt-H, it is considered that uniform Pt layers were prepared by the galvanic displacement reaction. The hollow structure observed in the TEM images and predominant Cu dissolution from FCC crystals suggests that the pores in the hollow nanoparticles mainly resulted from Cu atoms in the FCC crystals owing to the Kirkendall effect [22].

Compared to that of the $PdCu_2$ core, the crystal structure of $PdCu_2$-Pt-K was hardly changed by the Pt deposition process (Fig. 2b). Small changes in the crystal structure of $PdCu_2$-Pt-K may be attributed to limited Cu dissolution during the galvanic displacement process. Using ICP analysis, the utilization of the Pt precursor (mole of Pt deposited/mole of Pt introduced during the galvanic displacement process) in $PdCu_2$-Pt-K was calculated to be 21%, which is significantly lower than that in $PdCu_2$@Pt-H (78%) and $PdCu_2$-Pt-K-HCl (94%).

$PdCu_2$-Pt-K-HCl showed significant changes in crystal structure compared with the $PdCu_2$ core. The intensity of the diffraction peaks corresponding to BCC crystals are considerably decreased and the peak positions of the FCC crystal diffractions are negatively shifted from those of a $PdCu_2$ alloy to those of Pt (Fig. 2a and b). As the Pt contents in $PdCu_2$@Pt-H and $PdCu_2$-Pt-K-HCl are similar (Table S1), the large diffraction peak shifts in $PdCu_2$-Pt-K-HCl may be attributed to alloy formation between Pt and the $PdCu_2$ cores. In this case, it was presumed that the higher Cl^- concentration (around 8.3 mM) during the galvanic displacement process for $PdCu_2$-Pt-K-HCl led to easier dissolution of Cu

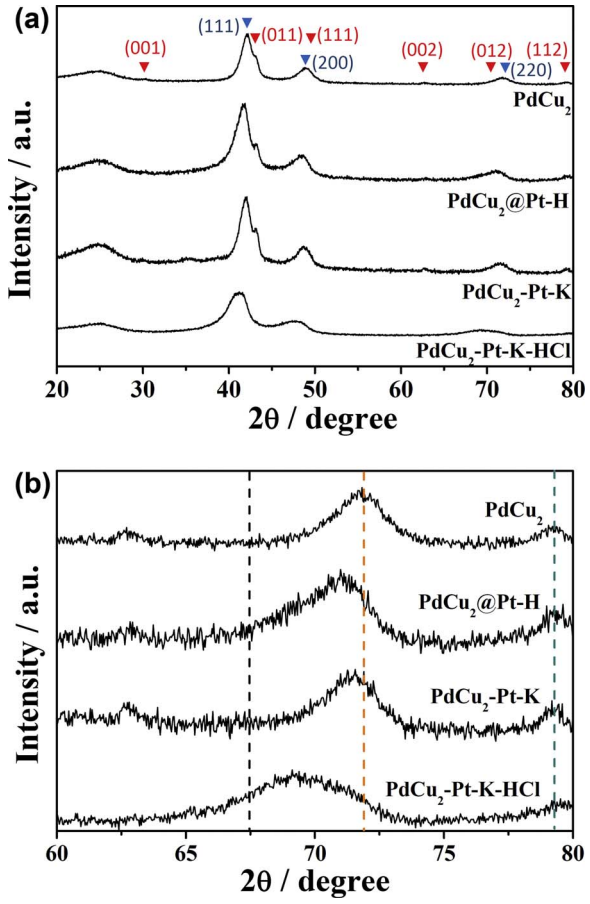

Fig. 2. (a) XRD patterns and (b) magnified XRD patterns (60–80°) of the electrocatalysts. Red and blue triangles in (a) indicate the diffraction peaks of FCC $PdCu_2$ and BCC PtCu, respectively. Black, orange, and blue dashed lines in (b) indicate the 2θ values of the (220), (220), and (112) diffractions of Pt, FCC $PdCu_2$, and BCC PdCu, respectively. (For interpretation of the references to colour in this figure legend, the reader is referred to the web version of this article.).

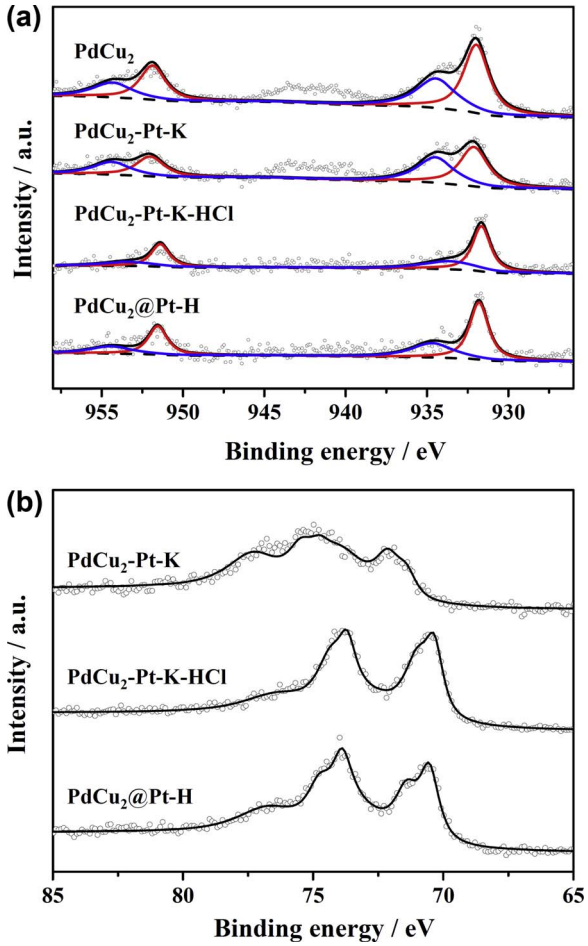

Fig. 3. (a) Cu 2p and (b) Pt 4f XPS spectra of the electrocatalysts.

and Pd. Then, as the standard reduction potential of Pd^{2+} is higher than that of Cu^{2+}, the galvanic displacement reaction of Cu with Pd^{2+} led to redeposition of dissolved Pd. A comparison of the crystal structures of $PdCu_2$@Pt-H and $PdCu_2$-Pt-K-HCl shows that the architecture of the $PdCu_2$@Pt nanoparticles is controlled by the Cl^- concentration as well as the pH.

From the comparison of $PdCu_2$, $PdCu_2$@Pt-H, $PdCu_2$-Pt-K-HCl, and $PdCu_2$-Pt-K-HCl, it was concluded that a high Cl^- (and K^+) concentration and low pH facilitate Cu dissolution and Pd dissolution, thereby leading to hollow structure formation. In contrast, high pH suppresses Pt deposition, probably owing to the formation of stable oxides. A high Cl^- concentration may result in dissolution occurring too quickly, with surface alloy formation accompanying redeposition of dissolved cores. Thus, to achieve an electrocatalyst with a hollow core and a uniform Pt shell via the galvanic replacement process, low pH and low Cl- and K^+ concentrations should be used for the Pt deposition process.

3.2. Effect of galvanic displacement conditions on the surface structure of the electrocatalysts

To investigate the chemical state of the surface atoms, XPS analysis was conducted (Fig. 3). The Cu 2p XPS spectrum of the $PdCu_2$ core nanoparticles shows peaks at 932.0 (Cu $2p_{3/2}$) and 951.9 eV (Cu $2p_{1/2}$) corresponding to metallic Cu and shoulder peaks at 933.6 and 954.2 eV corresponding to oxidized Cu (Fig. 3a) [23]. The peaks at approximately 942 and 962 eV are satellite peaks. After the galvanic displacement process, the Cu 2p XPS spectrum of $PdCu_2$-Pt-K is similar to that of the $PdCu_2$ cores, except that the area ratio of metallic Cu to oxidized Cu decreases from 1.53 to 1.20. In contrast, the area ratios for $PdCu_2$@Pt-H (1.88) and $PdCu_2$-Pt-K-HCl (1.95) increased, with reduced total peak areas and minor satellite peaks. This result implies that both oxidized and metallic Cu atoms were removed during the galvanic displacement process for the $PdCu_2$@Pt-H sample (acidic conditions), whereas the oxidized Cu atoms in $PdCu_2$-Pt-K (neutral conditions) were not removed, hindering the galvanic displacement process. This mechanism is plausible, as Cu^{2+} is the only stable species under acidic conditions, whereas both CuO and Cu_2O are stable under neutral conditions. The Pd 3d XPS spectrum of $PdCu_2$-Pt-K exhibits shoulder peaks at 336.1 and 341.4 eV, which indicate the presence of oxidized Pd atoms, such as PdO, whereas the $PdCu_2$ cores, $PdCu_2$-Pt-K-HCl, and $PdCu_2$@Pt-H only show metallic Pd atoms (Fig. S3) [23]. A comparison of the Pt 4f XPS spectra of $PdCu_2$@Pt-H, $PdCu_2$-Pt-K-HCl, and $PdCu_2$-Pt-K (Fig. 3b) also shows that the Pt atoms in $PdCu_2$-Pt-K are mainly Pt oxides, whereas those in $PdCu_2$@Pt-H and $PdCu_2$-Pt-K-HCl are metallic Pt [23]. Thus, the XPS analysis supports our conjecture that the galvanic displacement reaction using the K_2PtCl_6 precursor was hindered by surface oxides.

The surface properties of the electrocatalysts were investigated using cyclic voltammetry. The $PdCu_2$ nanoparticles exhibited little hydrogen adsorption/desorption behavior in the 0–0.4 V region and showed large anodic peaks at 0.41 and 0.65 V (Fig. 4a), which correspond to the dissolution of bulk Cu and underpotential deposition of Cu, respectively [24]. The dissolution peaks disappeared in the cyclic voltammograms of $PdCu_2$@Pt-H and $PdCu_2$-Pt-K-HCl (Fig. 4b). Moreover, the shape of the cyclic voltammograms of $PdCu_2$@Pt-H and $PdCu_2$-Pt-K-

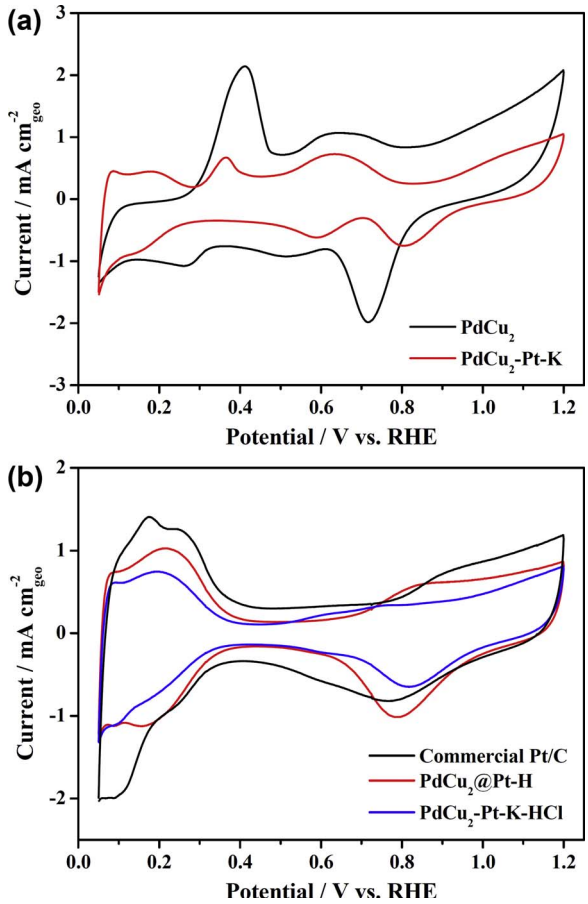

Fig. 4. (a) Cyclic voltammograms of $PdCu_2$ (black) and $PdCu_2$-Pt-K (red) and (b) cyclic voltammograms of $PdCu_2$@Pt-H (red), $PdCu_2$-Pt-K-HCl (blue), and commercial Pt/C (black). (For interpretation of the references to colour in this figure legend, the reader is referred to the web version of this article.).

HCl were similar to that of Pt/C, with hydrogen adsorption/desorption in the 0–0.4 V region, double layer charging/discharging in the 0.4–0.5 V region, and oxidation/reduction of Pt and/or Pd in the 0.6–1.2 V region. This behavior implies that the galvanic displacement process successfully replaced surface Cu with Pt in the $PdCu_2$@Pt-H and $PdCu_2$-Pt-K-HCl samples. In contrast, the Cu dissolution peaks were observed for $PdCu_2$-Pt-K, although the amplitude of the peaks was largely diminished. The observation of Cu dissolution peaks is in accordance with the low Pt concentration in $PdCu_2$-Pt-K, indicating incomplete deposition of a surface Pt layer. However, the decreased intensity is consistent with dissolution of 31% of the Cu atoms in $PdCu_2$-Pt-K during the galvanic displacement process, despite the low Pt deposition yield.

3.3. ORR activity and stability of the electrocatalysts

To evaluate the ORR activity of the electrocatalysts, we recorded their ORR polarization curves (Fig. 5a). As the amount of platinum group metals (PGM) on the working electrodes are different in each electrocatalyst, the kinetic currents determined using the polarization curves were normalized using the PGM mass (Fig. 5b) and surface area (Fig. 5c). The surface area was determined using the hydrogen desorption charge of the electrocatalysts and the charge density of hydrogen desorption on polycrystalline Pt (0.210 mC cm^{-2}). $PdCu_2$@Pt-H exhibited the highest PGM mass activity, followed by $PdCu_2$-Pt-K-HCl and then $PdCu_2$-Pt-K. At 0.9 V, where kinetic resistance is considered to be dominant, the mass activity of $PdCu_2$@Pt-H was 0.485 A mg^{-1}_{PGM}, which is 2.4 times higher than that of commercial Pt/C (0.201 A mg^{-1}_{PGM}). The mass activities of $PdCu_2$-Pt-K and $PdCu_2$-Pt-K-HCl at 0.9 V were 0.133 and 0.248 A mg^{-1}_{PGM}, respectively (Fig. 5d). The higher mass activity of $PdCu_2$@Pt-H compared with that of $PdCu_2$-Pt-K-HCl suggests that controlled displacement, resulting in surface Pt layers on an ordered intermetallic Pd–Cu core, and a hollow structure are crucial for efficient ORR electrocatalysis.

Fig. 5c gives the kinetic current normalized using the PGM surface area (specific activity) of the electrocatalysts. As the atomic sizes of Pd (0.137 nm) and Pt (0.139 nm) are similar, the specific activity reflects the turnover frequency of the electrocatalysts. The trend for the specific activity was similar to that of the mass activity, with the highest specific activity observed for $PdCu_2$@Pt-H and the lowest for $PdCu_2$-Pt-K. The high specific activity of $PdCu_2$@Pt-H is likely attributable to the unique architecture of $PdCu_2$@Pt-H, as the specific activity of $PdCu_2$-Pt-K-HCl is lower that of $PdCu_2$@Pt-H, but these samples have similar atomic compositions (Table S1). The major architecture differences between $PdCu_2$@Pt-H and $PdCu_2$-Pt-K-HCl are the crystalline structure (ordered intermetallic alloy maintained in $PdCu_2$@Pt-H) and surface structure (surface Pt layer formed in $PdCu_2$@Pt-H).

The stability of the $PdCu_2$@Pt-H electrocatalyst was evaluated by comparing the ORR polarization curves before and after potential cycling between 0.6 and 1.0 V for 10,000 cycles (Fig. 6a). The polarization curve of $PdCu_2$@Pt-H did not change considerably following potential cycling, indicating the excellent stability of this electrocatalyst. Under the same conditions, the polarization curve of commercial Pt/C showed a negative shift of 6 mV and a decrease in mass activity by 14.7%. Though the mild potential cyclic conditions (0.6–1.0 V) seemed to limit cathodic dissolution of Pt during potential cycling [25], resulting in relatively slow degradation of the Pt/C electrocatalysts, the distinct differences in the polarization curves emphasize the high stability of the $PdCu_2$@Pt-H electrocatalyst. The excellent stability of the $PdCu_2$@Pt-H electrocatalyst seems to be due to its unique structure, i.e., Pt layers on an ordered intermetallic Pd–Cu core. As the major contribution to the degradation of alloy electrocatalysts is dissolution of transition metals, the limited dissolution of Cu in the ordered intermetallic BCC crystal during galvanic displacement supports the suggestion that the ordered intermetallic Pd–Cu cores are beneficial for durable electrocatalysts.

The cyclic voltammogram of $PdCu_2$@Pt-H after potential cycling showed decreased hydrogen adsorption/desorption behavior and oxidation/reduction of Pd/Pt (Fig. 6b), whereas little degradation of the ORR activity was observed in the polarization curves. As the polarization curve is governed by the surface area and specific activity, small changes in the polarization curve and decreased surface area result in enhanced specific activity. The enhanced specific activity may be attributed to the reduced oxygen binding energy. The anodic scan of the cyclic voltammogram shows that the oxidation of Pd/Pt is retarded by approximately 40 mV after potential cycling. Enhanced specific activity accompanying retarded oxidation of a Pt alloy has been well elucidated by Stamenkovic et al. using a Pt–Ni alloy electrocatalyst [26]. In our electrocatalysts, the retarded oxidation is believed to originate from the rearrangement of surface atoms [22]. There are several possible reasons for the enhanced specific activity after potential cycling. One plausible reason is smoothing of the Pt shell, *i.e.*, removal of defect sites such as steps, adatoms, and kinks. As the ORR activities of defect sites are significantly lower than those of basal planes, such as (111) facets, smoothing of nanoparticle surfaces by potential cycling would enhance the ORR activity [27]. Moreover, structural changes caused by segregation of core atoms may alter the surface structure of $PdCu_2$@Pt-H electrocatalysts. Similar to the enhanced specific activity of Pd–Au@Pt core–shell nanoparticles after potential cycling reported by Cai et al. [27] and in our previous study [28], the Cu atoms in $PdCu_2$@Pt-H may be segregated to surfaces during cycling. This phenomenon would enhance the ORR activity of the Pt shell owing to increased lattice contraction via surface alloying of the Pt shell with Cu.

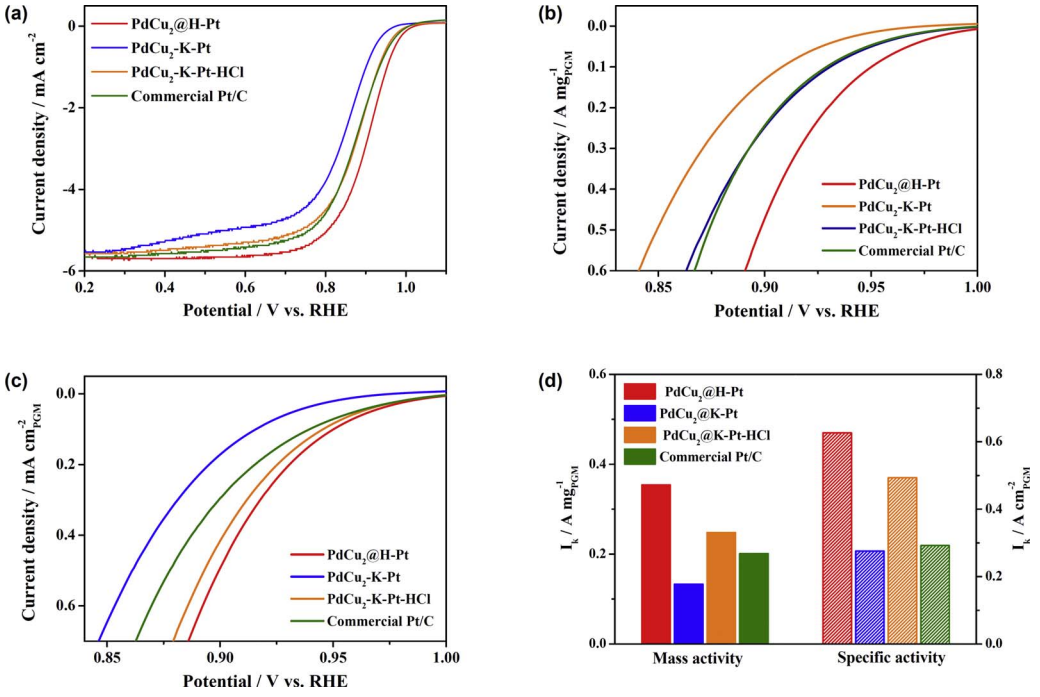

Fig. 5. (a) ORR polarization curves of the electrocatalysts, (b) PGM mass specific kinetic current densities, (c) PGM surface area specific current densities, and (d) mass (left) and area (right) specific activities measured at 0.9 V.

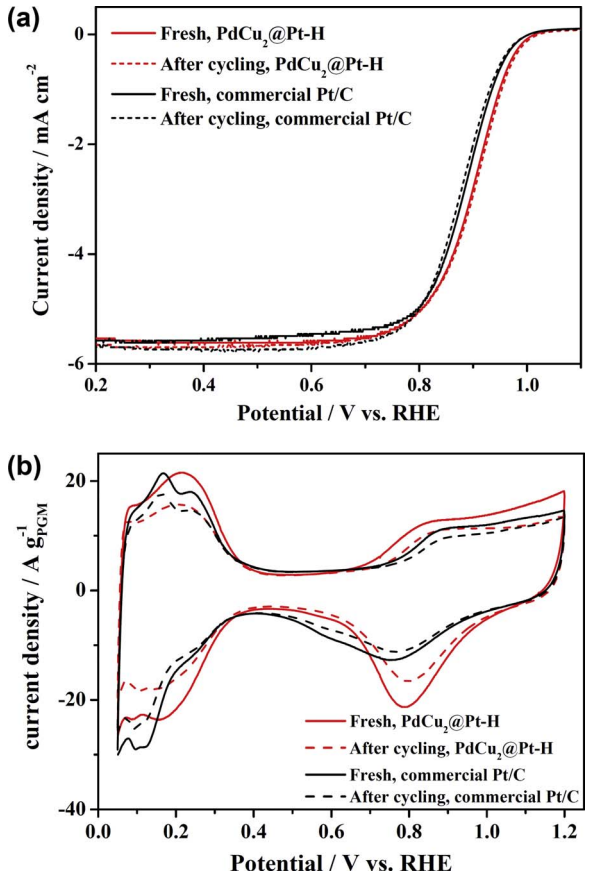

Fig. 6. (a) ORR polarization curves and (b) cyclic voltammograms of $PdCu_2$@Pt-H (red) and commercial Pt/C (black) electrocatalysts before (solid lines) and after (dashed lines) potential cycling for 10,000 cycles. (For interpretation of the references to colour in this figure legend, the reader is referred to the web version of this article.).

4. Conclusion

Using a galvanic displacement process, hollow $PdCu_2$@Pt core@shell nanoparticle electrocatalysts were prepared. The $PdCu_2$ cores have an ordered intermetallic structure that seems to be beneficial for the stability of the electrocatalysts. To achieve uniform Pt layers rather than surface alloys, low pH conditions that hinder or remove surface oxides and a low anion concentration, i.e., ionic strength, are required during the galvanic displacement process. By combining these two factors, the highly active and stable $PdCu_2$@Pt-H electrocatalyst was obtained. We believe that this research contributes a simple and robust synthesis to control the architecture of Pt layers on hollow nanoparticles for electrocatalysis in PEMFCs.

Conflict of interest

The authors declare no competing financial interest.

Acknowledgement

This work was supported financially by the Global Frontier R Program on Center for Multiscale Energy System (2016M3A6A7945505), an NRF grant funded by MSIP (2017R1A2B2003363, 2015R1A2A2A01007622), the KIST Institutional Program, and the New and Renewable Energy Core Technology Program of KETEP grant funded by MOTIE (20143030031340).

Appendix A. Supplementary data

Supplementary data associated with this article can be found, in the online version, at https://doi.org/10.1016/j.apcatb.2017.11.052.

References

[1] B. Han, C.E. Carlton, A. Kongkanand, R.S. Kukreja, B.R. Theobald, L. Gan, R. O'Malley, P. Strasser, F.T. Wagner, Y. Shao-Horn, Energy Environ. Sci. 8 (2015) 258–266.
[2] I.E.L. Stephens, A.S. Bondarenko, U. Gronbjerg, J. Rossmeisl, I. Chorkendorff, Energy Environ. Sci. 5 (2012) 6744–6762.
[3] J. Greeley, I.E.L. Stephens, A.S. Bondarenko, T.P. Johansson, H.A. Hansen, T.F. Jaramillo, J. Rossmeisl, I. Chorkendorff, J.K. Nørskov, Nat. Chem. 1 (2009)

552–556.
[4] V.R. Stamenkovic, B.S. Mun, K.J.J. Mayrhofer, P.N. Ross, N.M. Markovic, J. Am. Chem. Soc. 128 (2006) 8813–8819.
[5] Y. Xing, Y. Cai, M.B. Vukmirovic, W.-P. Zhou, H. Karan, J.X. Wang, R.R. Adzic, J. Phys. Chem. Lett. 1 (2010) 3238–3242.
[6] M.B. Vukmirovic, J. Zhang, K. Sasaki, A.U. Nilekar, F. Uribe, M. Mavrikakis, R.R. Adzic, Electrochim. Acta 52 (2007) 2257–2263.
[7] J. Zhang, M.B. Vukmirovic, Y. Xu, M. Mavrikakis, R.R. Adzic, Angew. Chem. Int. Edn. 44 (2005) 2132–2135.
[8] K. Sasaki, J.X. Wang, H. Naohara, N. Marinkovic, K. More, H. Inada, R.R. Adzic, Electrochim. Acta 55 (2010) 2645–2652.
[9] T. Cochell, A. Manthiram, Langmuir 28 (2012) 1579–1587.
[10] M. Shao, K. Shoemaker, A. Peles, K. Kaneko, L. Protsailo, J. Am. Chem. Soc. 132 (2010) 9253–9255.
[11] N. Jung, Y. Sohn, J.H. Park, K.S. Nahm, P. Kim, S.J. Yoo, Appl. Catal. B: Environ. 196 (2016) 199–206.
[12] B.I. Podlovchenko, T.D. Gladysheva, A.Y. Filatov, Mendeleev Commun. 25 (2015) 293–295.
[13] T. Cochell, W. Li, A. Manthiram, J. Phys. Chem. C 117 (2013) 3865–3873.
[14] J. Zhang, Y. Mo, M.B. Vukmirovic, R. Klie, K. Sasaki, R.R. Adzic, J. Phys. Chem. B 108 (2004) 10955–10964.
[15] A.-R. Park, Y.-W. Lee, D.-H. Kwak, K.-W. Park, Korean J. Chem. Eng. 32 (2015) 1075–1080.
[16] J. Ryu, J. Choi, D.-H. Lim, H.-L. Seo, S.-Y. Lee, Y. Sohn, J.H. Park, J.H. Jang, H.-J. Kim, S.A. Hong, P. Kim, S.J. Yoo, Appl. Catal. B: Environ. 174–175 (2015) 526–532.
[17] Z. Cui, H. Chen, W. Zhou, M. Zhao, F.J. DiSalvo, Chem. Mater. 27 (2015) 7538–7545.
[18] T. Tamaki, A. Minagawa, B. Arumugam, B.A. Kakade, T. Yamaguchi, J. Power Sources 271 (2014) 346–353.
[19] D. Wang, H.L. Xin, R. Hovden, H. Wang, Y. Yu, D.A. Muller, F.J. DiSalvo, H.D. Abruña, Nat. Mater. 12 (2013) 81–87.
[20] B. Beverskog, I. Puigdomenech, J. Electrochem. Soc. 144 (1997) 3476–3483.
[21] P.R. Subramanian, D.E. Laughlin, J. Phase Equilib. 12 (1991) 231–243.
[22] J.X. Wang, C. Ma, Y. Choi, D. Su, Y. Zhu, P. Liu, R. Si, M.B. Vukmirovic, Y. Zhang, R.R. Adzic, J. Am. Chem. Soc. 133 (2011) 13551–13557.
[23] W.M.R.C.D. Wagner, L.E. Davis, J.F. Moulder, G.E. Muilnenberg, Handbook of x-ray Photoelectron Spectroscopy: A Reference Book of Standard Data for Use in x-ray Photoelectron Spectroscopy, Physical Electronics Division, Perkin-Elmer Corp., Eden Prairie, 1979.
[24] A. Kumar, D.A. Buttry, J. Phys. Chem. C 119 (2015) 16927–16933.
[25] A.A. Topalov, S. Cherevko, A.R. Zeradjanin, J.C. Meier, I. Katsounaros, K.J.J. Mayrhofer, Chem. Sci. 5 (2014) 631–638.
[26] V.R. Stamenkovic, B. Fowler, B.S. Mun, G. Wang, P.N. Ross, C.A. Lucas, N.M. Marković, Science 315 (2007) 493–497.
[27] Y. Cai, C. Ma, Y. Zhu, J.X. Wang, R.R. Adzic, Langmuir 27 (2011) 8540–8547.
[28] S.-Y. Lee, N. Jung, D.Y. Shin, H.-Y. Park, D. Ahn, H.-J. Kim, J.H. Jang, D.-H. Lim, S.J. Yoo, Appl. Catal. B: Environ. 206 (2017) 666–674.